POTENTIAL APPLICATIONS OF THE SENTINEL-2 MULTISPECTRAL SENSOR AND THE ENMAP HYPERSPECTRAL SENSOR IN MINERAL EXPLORATION

Christian Mielke[1], Nina Kristine Bösche[1], Christian Rogass[1], Karl Segl[1], Christoph Gauert[2], and Hermann Kaufmann[1]

1. Helmholtz Zentrum, GFZ German Research Centre for Geosience, Potsdam, Germany; {christian.mielke/nina.boesche/christian.rogass/karl.segl/hermann.kaufmann}(at)gfz-potsdam.de
2. Department of Geology, University of the Free State (UFS), Bloemfontein 9300, South Africa; gauertcdk(at)ufs.ac.za

ABSTRACT

Imaging spectroscopy is a widely used tool in mineral exploration today where exploration companies offer the full service package to their clients: (data acquisition, preprocessing and product delivery). These exploration projects rely mainly on airborne imaging spectrometers such as Hymap, AISA or HySpex. This data is usually scarce and expensive and may not be available to academic research. The only operational spaceborne imaging spectrometer that covers the full spectral range from the visible to the shortwave infrared is Hyperion aboard EO-1, which has been providing data for over a decade now. New and advanced spaceborne imaging spectrometers such as the Environmental Mapping and Analysis Program (EnMAP) will provide new data for research in the field of imaging spectroscopy for mineral exploration. This study presents a comparison of the mapping capabilities between the Hyperion and EnMAP sensors, on the basis of simulated EnMAP data. This is shown with an example from a porphyry copper complex in southern Namibia (Haib River). Results from multispectral sensors (Landsat-8 OLI, EO-1 ALI and simulated data from the next generation Sentinel-2) are shown to illustrate their potential to map the gossan-outcrops at the Haib River Complex using the Iron Feature Depth (IFD).

INTRODUCTION

The use of airborne hyperspectral imaging spectrometers such as HyMAP (1) or HySpex (2) is a common approach in exploration campaigns today (3). These airborne sensors combine a good signal-to-noise ratio and a good spectral and spatial resolution. However, the usage of these systems in large and remote areas involves high costs due to the difficult logistics that is involved in airborne hyperspectral campaigns. Therefore, the usage of multispectral imagers, such as the Operational Land Imager aboard Landsat-8 (4) and Sentinel-2 (5) in combination with hyperspectral spaceborne instruments such as Hyperion (6) and EnMAP(7), will increase in geological mapping and exploration campaigns to reduce airborne related costs to a minimum possible extent. This is due to the open data policy that accompanies these spaceborne missions as in the case of the National Aeronautics and Space Administration's (NASA's) EO-1 satellite, or NASA's Landsat programme. The future European Sentinel-2 and the future German EnMAP missions will supply data with a similar data usage policy to the geoscientific community worldwide. Therefore, the study presented here aims at illustrating synergetic effects in mineral exploration that emerge from the usage of these spaceborne multispectral and hyperspectral instruments. This is done for the Haib River porphyry copper deposit in the lower Orange River area, shown in Figure 1, which has been identified as one of the oldest porphyry copper deposits in the world (8,9) situated in the Namaqua Mobile Belt (10). Early exploration work before the work of Minnit (9) is advocating for a classical succession of hydrothermal alteration zones, which indicate a porphyry copper deposit (9). Through fieldwork and stable isotope work Barr and Reid (11) found that a classical alteration zonation as proposed by Minnit (9) cannot be readily identified due to two phases of hydrothermal activity that were overprinting each other in host rocks that had already been altered to lower

DOI: 10.12760/01-2014-2-07

greenschist facies. The presence of gossans in the field on mineralized rocks, such as the Haib River quartz-feldspar porphyry, the nearby sericitic alteration and the associated clay- and alteration-mineralogy show spatially distinct patterns near the ore zone, which can serve as exploration indicators that focus on future and more detailed field- and airborne-exploration campaigns. Therefore, this area represents a unique test site for the demonstration of new remote sensing techniques for mineral mapping and exploration (12) and for a demonstration of the synergetic and complementary use of multispectral- and hyperspectral-spaceborne data in exploration.

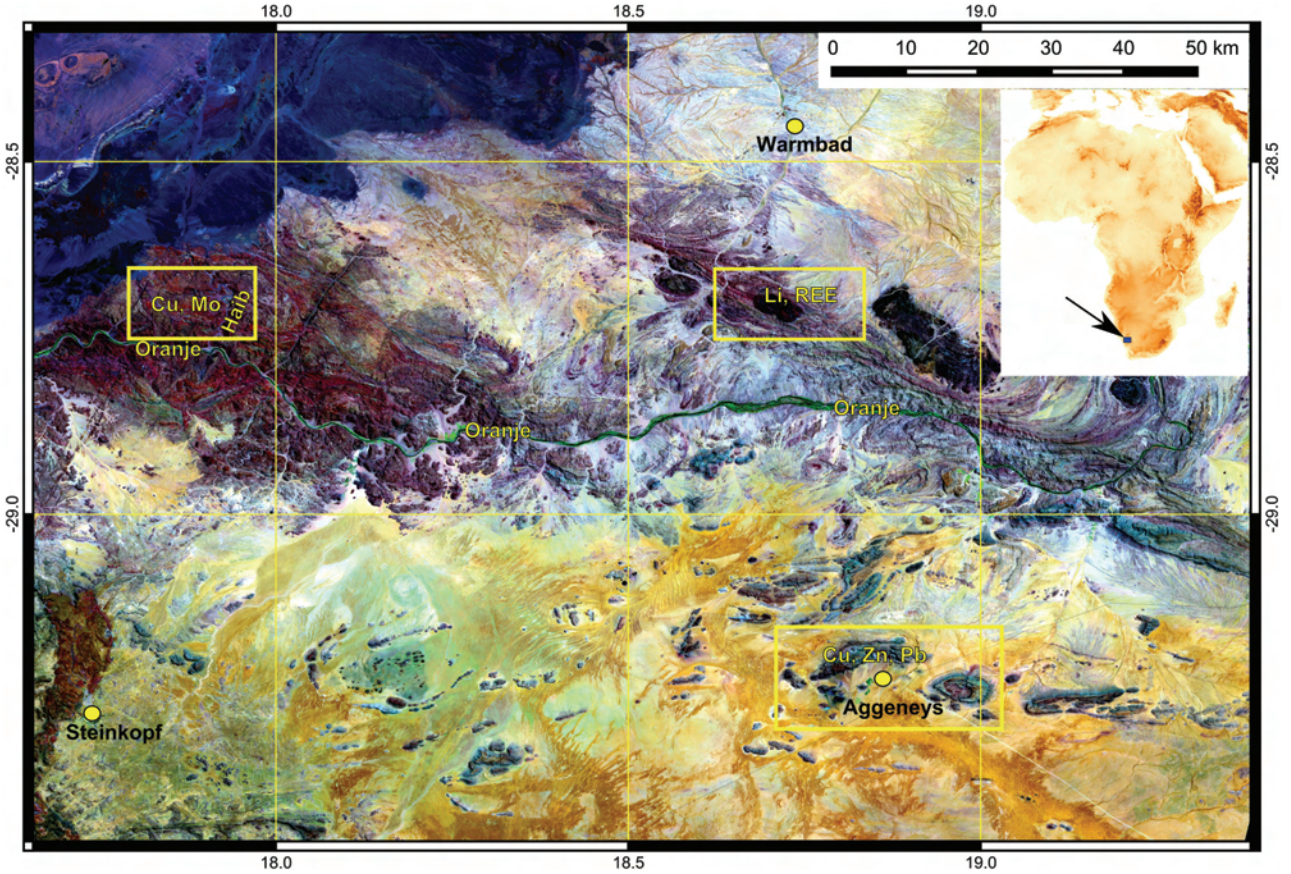

Figure 1: Landsat-8 OLI false colour composite (OLI scene ID: LC81760802014026LGN00) (R: 2200 nm, G: 860 nm, B: 560 nm) showing the Orange River area with the three major mineral deposit sites in the border region of South Africa and Namibia. These are the Aggeneys lead-zinc deposit, the lithium pegmatites and rare earth element bearing site close to Tantalite Valley, south of Warmbad and the Haib River Complex with its copper deposit. Topographic map from ETOPO-1 data showing the location of the lower Orange River area.

METHODS

For this study data was acquired from the EO-1 Hyperion and ALI sensors, as well as data from Landsat-8 OLI, shown in Figure 1. Airborne hyperspectral data (HyMAP) from the Geological Survey of Namibia was used to simulate the future multispectral Sentinel-2 and the future hyperspectral EnMAP sensor using the EnMAP End-to-End simulation tool of Segl et al. (13). This tool enables the demonstration of the full capacity of Sentinel-2 and EnMAP by a full forward and backward simulation, which includes the simulation of EnMAP-like and Sentinel-2-like raw data from spatially and spectrally higher resolved airborne data (forward simulation) and the succeeding preprocessing of the synthetic sensor data to at-ground-reflectance (backward simulation) (13). The now derived, simulated reflectance data facilitates algorithm development for scientific data exploitation and validation prior to the launch of these two sensors.

Fieldwork was carried out for sample collection and field spectrometer measurements for verification purposes that were carried out in a sensor adapted way that mimics the sensors Point-Spread-Function (PSF) in the field by a Gaussian weighting of 17 defined test surfaces (nine test surfaces for the central EnMAP and Sentinel-2 pixel and eight test surfaces in the centres of the eight neighbourhood pixels). This technique has been used and described in detail in mine waste related field work (14,15). The resulting spectrum is then resampled to the according spectral resolution of the multispectral sensors using a convolution of the sensor specific Gaussian filter functions with the PSF weighed spectrum. The outcome of this process is shown in Figure 2 from a test site in the western gossan area, shown in Figure 3.

Table 1: Sensor coverage for EnMAP, Sentinel-2 and the hyperspectral sensor that was used to simulate the two datasets (HyMAP).

Sensor	Centre wavelength first band (nm)	Centre wavelength last band (nm)
HyMAP	439	2484
EnMAP	423	2439
Sentinel-2	442	2189

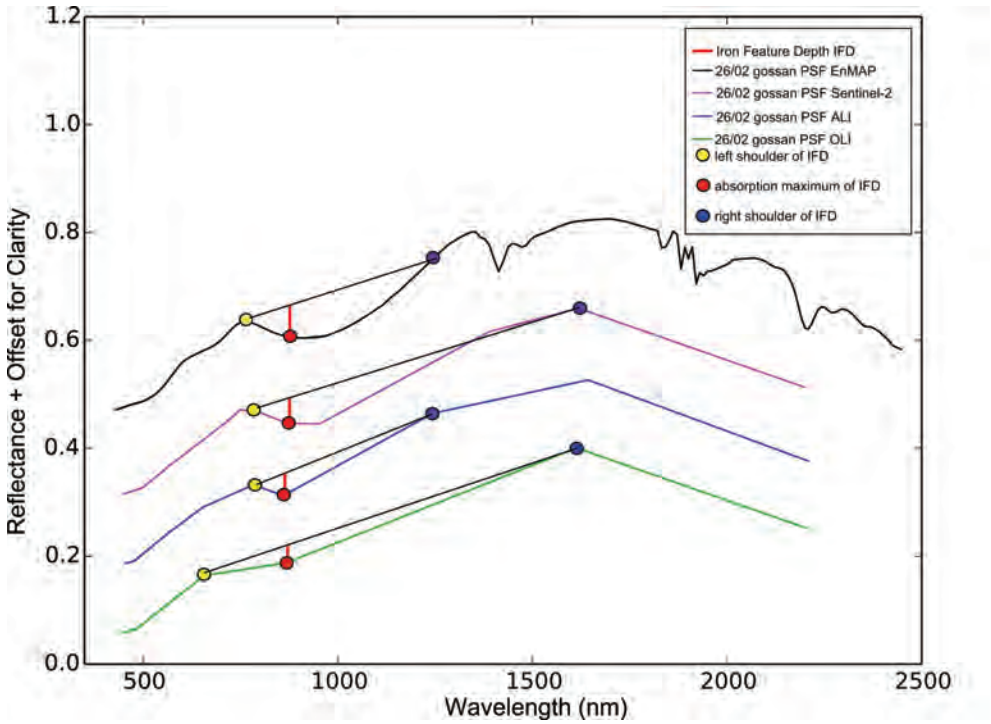

Figure 2: Definition of the Iron Feature Depth for selected multispectral sensors (hyperspectral EnMAP data for reference) to illustrate the capacity of the IFD for mapping the iron absorption feature in a spectrum from the Haib River Complex.

In order to exploit the large spatial coverage of multispectral spaceborne instruments the Iron Feature Depth (IFD) (15) is used for mapping the spatial distribution of secondary iron bearing minerals such as goethite, hematite and jarosite. These minerals are essential in the process of exploration, where the occurrence of gossans may show zones of sulfide oxidation and metal leaching, which can be indicative for copper exploration (16) and material transport from mine waste sites (15). Figure 2 shows the IFD, which exploits the 900 nm iron absorption feature in a three-point band-depth fashion. Here the left shoulder (yellow dot in Figure 2) is represented by the sensor channel closest to 750 nm, the right shoulder (blue dot in Figure 2) is represented as the SWIR 1 channel closest to 1250 nm, excluding sensor bands that include the water vapour absorption feature at 1380 nm. A linear interpolation is carried out between these shoulder points. The difference

between the linear interpolated sensor value closest to the 900 nm iron absorption feature and the measured sensor value gives the IFD (15). The IFD can be used to outline areas, which are covered with primary and secondary iron bearing minerals, as in case of the gossan areas shown in Figure 3. Even OLI is able to map the iron related absorption feature at 900 nm due to its band layout, as shown in Figure 2 indicating the presence of a gossan surface. Hyperspectral spaceborne data in combination with the USGS Mineral Identification and Characterization Algorithm (MICA) was used (17) for mapping the mineral distribution of the alteration minerals from the hyperspectral spaceborne data, which complements the IFD analysis of the multispectral spaceborne systems, which only have one spectral channel beyond 2000 nm, except for the Advanced Spaceborne Thermal Emission and Reflection Radiometer (ASTER) (18).

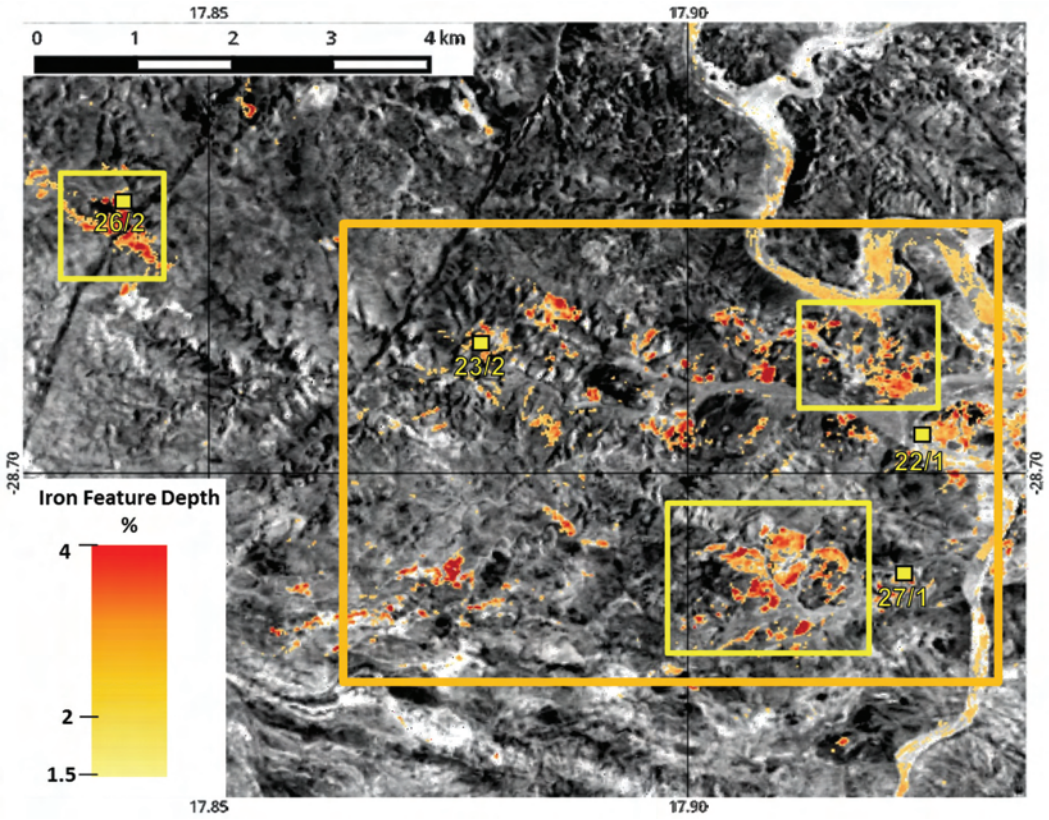

Figure 3: Iron Feature Depth (IFD) calculated from simulated Sentinel-2 data for the central part of the Haib River Complex; the orange box roughly outlines the zone of main mineralization, whilst the yellow boxes outline areas, which are covered by gossans. These yellow areas represent important anomalies, which also need to be considered in further exploration work. Yellow squares outline test sites of PSF validation measurements in the field.

RESULTS

Figure 4 shows IFD results calculated from test sites that have been measured in a sensor adapted PSF pattern. We see that the largest IFD values can be calculated from data that has been resampled to the spectral resolution of EnMAP, Sentinel-2 and ALI, which corresponds well with the ability of the different sensors to characterize the iron absorption feature at 900 nm, as shown in Figure 2 and as reported in (15).

Figure 4 shows that test site 26/2 has the highest IFD values if compared to the IFD values of 23/2, 27/1 and 22/1. Field samples of test site 26/2 of hand specimen size were scanned in the GFZ Spectral Laboratory using the state of the art imaging spectrometers: HySpex VNIR-1600 and the HySpex SWIR-320 m-e, fixed mounted at NADIR view over a translation stage. The illumination source is a 2000 W Hedler studio light.

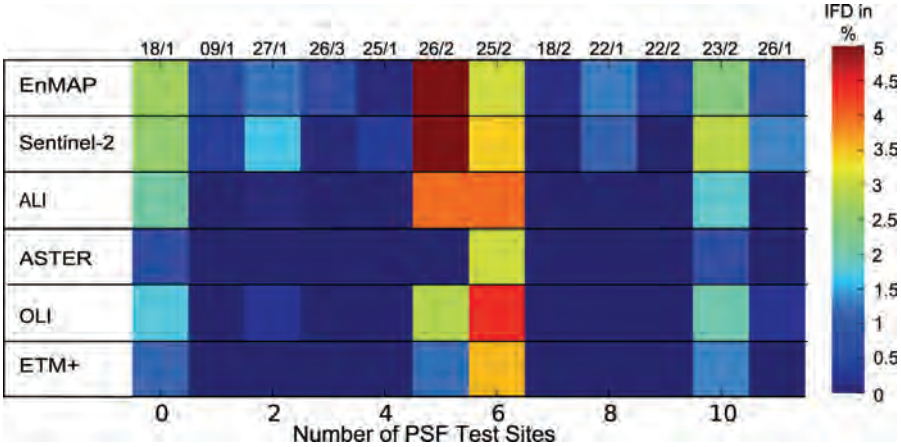

Figure 4: Iron Feature Depth (IFD) calculated from PSF weighed and spectrally resampled ASD field-spectrometer data. Test surface 18/1 and 09/1 are malachite and gossan bearing PSF test sites from exploration work near Opuwo northern Namibia, shown for comparison.

Figure 5 shows co-registered spectra from the HySpex laboratory scene shown as RGB inset map. Here we see an interesting effect that can be described as “spectral muting” of the iron absorption features in the visible and near infrared. The darker iron crusts exhibit lower IFD values due to the depression of the local maxima (left shoulder) of the iron absorption feature. This fact leads to a lower interpolated absorption near 900 nm and thus to a lower IFD value. This is shown in the cyan spectrum, which can be compared to the green spectrum that exhibits a much deeper iron absorption feature around 900 nm.

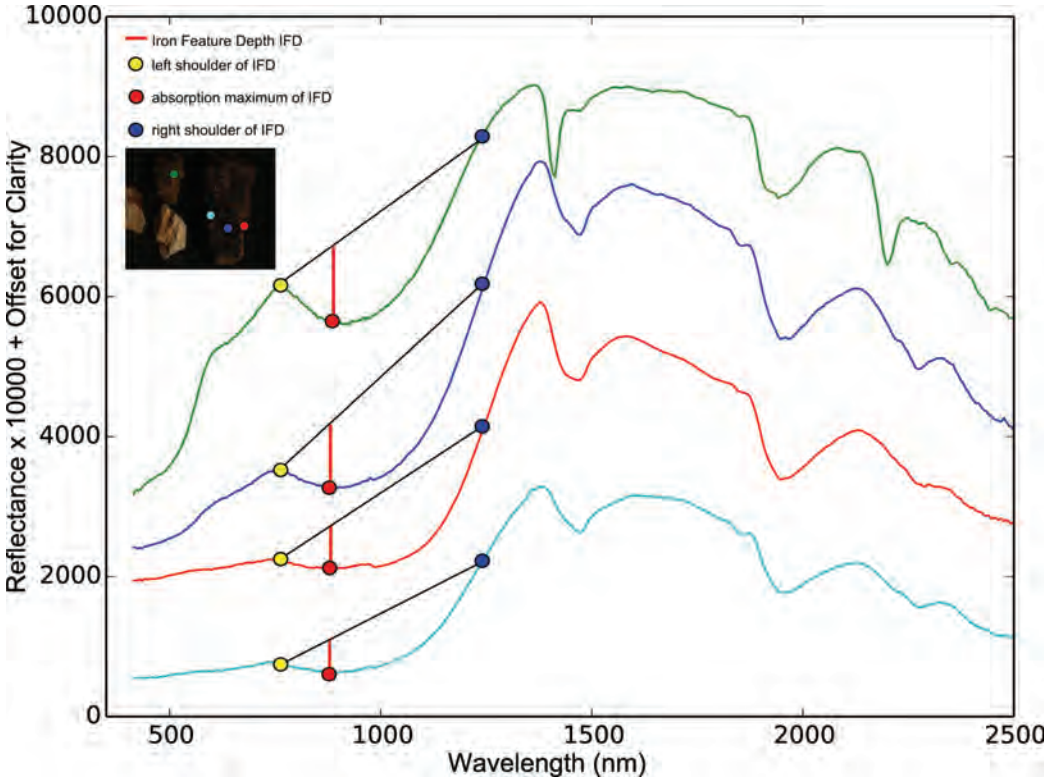

Figure 5: Iron Feature Depth (IFD) shown on spectra from a HySpex laboratory scan shown as small RGB composite inset map in the legend of the figure. Coloured spectra correspond to the locations of the coloured dot markers on the inset figure.

Figure 6 shows IFD images calculated of samples from test-site 26/2 scanned with the HySpex in the GFZ spectral laboratory. The HySpex laboratory data has been spectrally resampled to the spectral response of the multispectral sensors, prior to the calculation of the IFD. Here we see the

above mentioned difference in the quality of the different multispectral sensors to quantify the IFD via the 900 nm iron absorption. ASTER and Landsat-7 ETM+ perform least in characterizing the gossan surface, whilst Sentinel-2, ALI and OLI perform well in resolving the differences in the IFD of the sample. Remarkable is also the close similarity in the spatial pattern of the IFD on the Sentinel-2, ALI and OLI samples. This shows that these sensors are the most suitable instruments to map the spatial distribution of gossan patterns via the IFD.

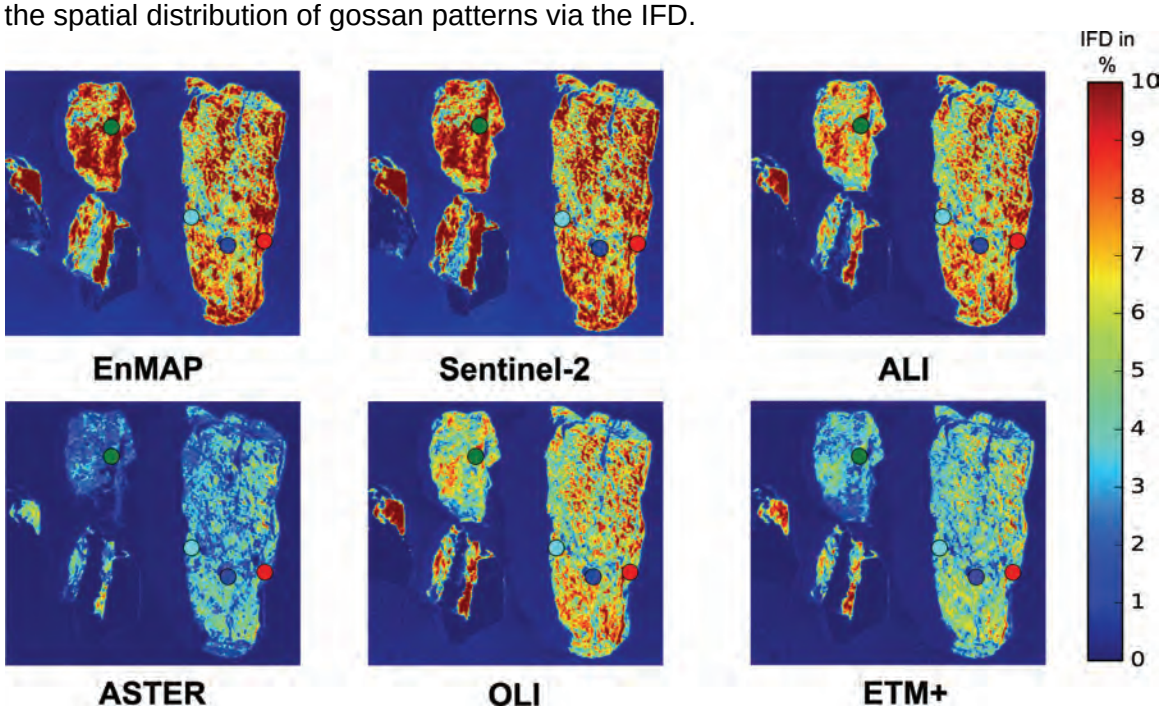

Figure 6: Iron Feature Depth (IFD) calculated from spectrally resampled HySpex laboratory measurement of hand specimens of gossan material from test site 26/2. Please note the difference in the ability of the multispectral sensors to map the IFD according to sensor characteristics (central wavelength and full width at half maximum).

Another interesting fact is that “spectrally muted” IFD areas, areas with a darker more mature gossan cover, show lower IFD values than their corresponding neighbours. This fact may be exploited in area wide multispectral data takes, shown in Figure 7. Here the spatial distribution of the IFD for Sentinel-2, ALI and OLI is shown. The spatial patterns of the IFD are very similar between the three sensors in Figure 7. The reason why the north-westernmost gossan area is not captured by ALI IFD result is due to the data extent of ALI. The ALI data only covers the central part of the Haib Complex. OLI, however, is able to show this north-westernmost gossan area despite its lower capability to quantify gossan surfaces in comparison to EnMAP, Sentinel-2 and ALI, shown above in Figure 6. Another important aspect is the ability of next generation multispectral sensors such as Sentinel-2 to discriminate between different secondary iron phases from the USGS digital spectral library (19), shown in comparison to EnMAP data in Figure 8. It is possible to see differences in the shape of the 900 nm iron absorption feature due to the higher spectral resolution of Sentinel-2 in the red and near-infrared part of the spectrum if compared to other multispectral instruments, such as ALI or OLI. This fact may be exploited to characterize the spectrum of 26/2 as a goethite dominated mixture of the secondary iron minerals, shown in Figure 8.

Hyperspectral spaceborne data from EO-1 Hyperion and from simulated EnMAP data complements the analysis from the multispectral spaceborne sensors and their IFD pattern by showing the spatial distribution of minerals that highlight zones of alteration mineralogy. These zones are outlined by yellow and blue boxes in Figure 9, where typical alteration minerals such as alunite, kaolinite and montmorillonite have been detected via the USGS MICA analysis (17). The spatial co-occurrence between the clay mineral anomaly in the blue boxes and the westernmost IFD area suggests a mineralogical exploration anomaly that needs to be evaluated by further exploration work in the field.

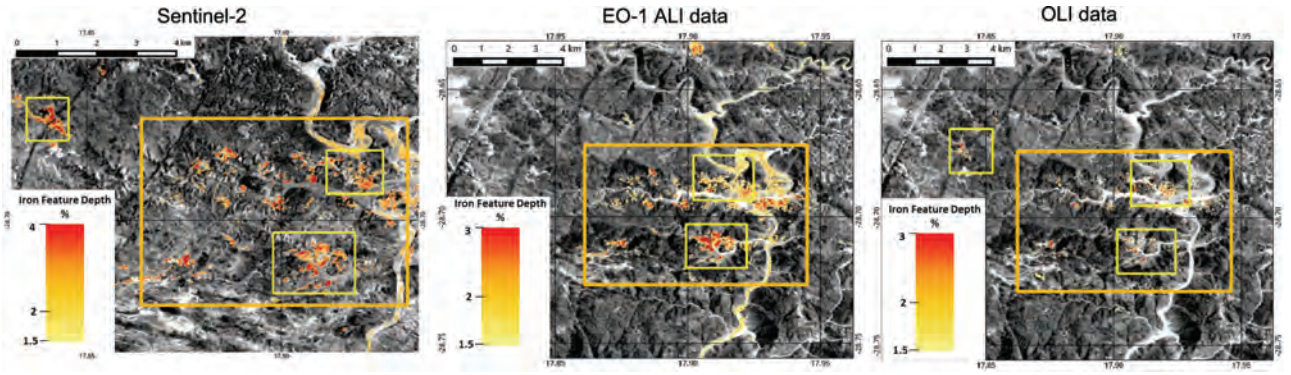

Figure 7: Iron Feature Depth calculated from simulated Sentinel-2 data, from EO-1 ALI (ALI scene IDs: EO1A1760802013267110K, EO1A1760802014013110PF) and from Landsat-8 OLI, (OLI scene ID: LC81760802014026LGN00) overlain over the Landsat-8 OLI near-infrared channel. Yellow boxes outline the occurrences of gossans, whilst the orange box outlines the main mineralized zone of the ore deposit.

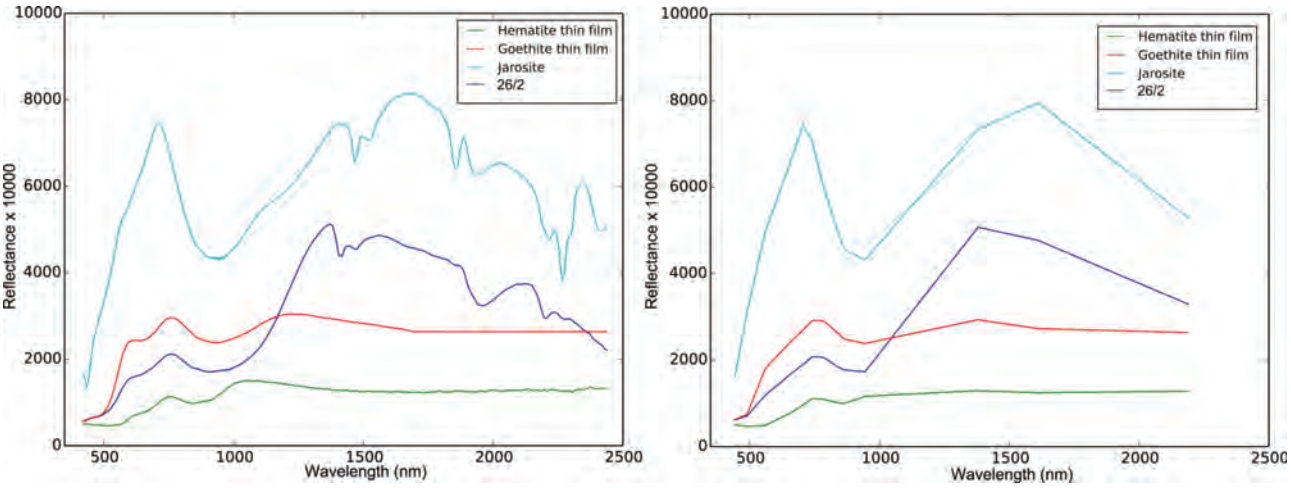

Figure 8: Mineral spectra from the USGS digital spectral library versus a spectrum from the aforementioned HySpex hand-specimen scan, resampled to the spectral resolution of EnMAP (left) and Sentinel-2 (right).

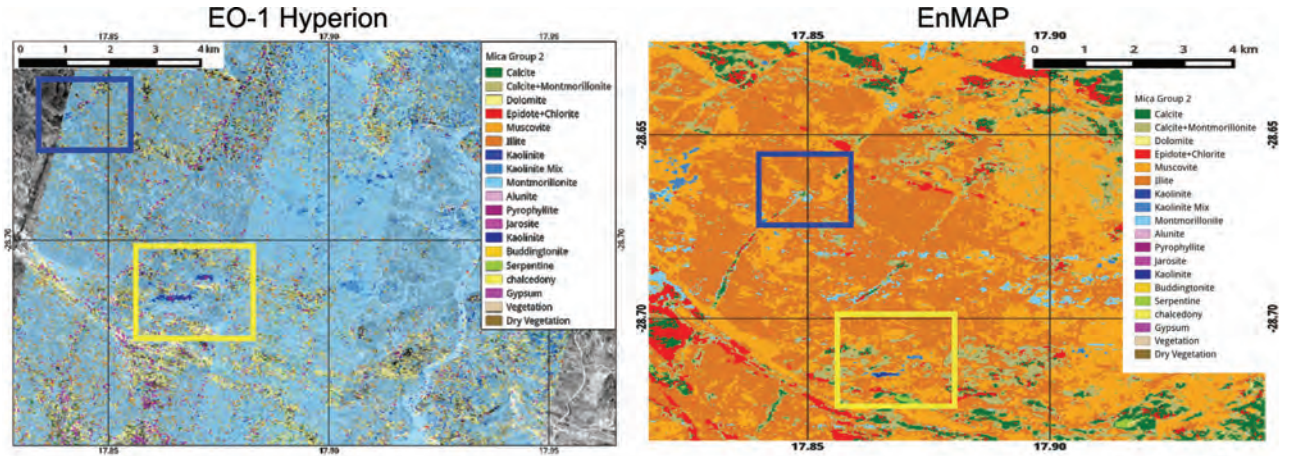

Figure 9: USGS MICA group 2 analysis results highlighting alteration zones within the Haib River Complex (yellow boxes). Analysis were carried out on EO-1 Hyperion data (Hyperion scene IDs: EO1H1760802013267110K, EO1H1760802014013110PF). Please note that the clay mineral occurrence in the Hyperion data and in the simulated EnMAP data (blue boxes) spatially coincides with the IFD anomaly in Figure 3 on the Sentinel-2 and OLI data on the westernmost dike structure.

CONCLUSIONS

This study showed that a combined, complementary use of multi- and hyperspectral spaceborne data yields high potential for mineral exploration. The spatial occurrence of gossans can be mapped from multispectral spaceborne data using the IFD (15) as demonstrated in Figures 3, 6 and 7. Next generation multispectral data may even be capable to highlight the dominant secondary iron mineral, such as goethite in case of the spectrum shown in Figure 8. This may help to establish a further subdivision of the gossans via their IFD and other additional criteria from next generation multispectral sensors such as Sentinel-2. This could be achieved through further more focused research on metal-sulfide oxidation, spaceborne imaging spectroscopy and ore deposits, which may then discriminate gossans formed by the oxidation of pyrite from those gossans dominated by the oxidation of copper bearing sulfides e.g. chalcopyrite (16). Hyperspectral spaceborne data is then able to further highlight zones of alteration mineralogy, if analyzed with expert systems, such as the USGS MICA (17). This combination of potential gossan anomalies and alteration mineralogy then yields important target zones for further exploration work, which may include high spatial resolution hyperspectral airborne data takes and identification of zones for further field investigations. This can then help to locate the zones of potential sulfide oxidation (zones of high secondary iron mineral abundance and hence zones with a strong positive IFD) and supergene copper enrichment (16).

The differences in the MICA analysis between the simulated EnMAP data and Hyperion are due to the generally lower, unfavorable signal-to-noise ratio of Hyperion if compared to the high signal-to-noise ratio of EnMAP. However both sensors show the two elliptical alteration mineral anomalies outlined in the yellow boxes of Figure 9. This shows that a combination of next generation multispectral sensors, such as the Sentinel-2 for gossan detection via the IFD and next generation hyperspectral sensors, such as EnMAP for identification of alteration mineralogy and mapping will likely reduce costs in future exploration campaigns by further focusing expensive airborne hyperspectral campaigns and field work on potential target areas that have been highlighted and interpreted as mineralogical exploration anomalies of interest.

ACKNOWLEDGEMENTS

Thanks to the Geological Survey of Namibia, Gaby Schneider and Ivor Kahimise for providing the Haib River HyMAP survey as EnMAP simulation input. Thanks to Stuart Frye and the EO-1 science team for providing the data takes of EO-1 ALI and Hyperion. Special thanks to the USGS and NASA Landsat-8 science team for providing the Landsat data. Special thanks to the National Oceanic and Atmospheric Administration (NOAA) for providing the ETOPO-1 data.

This work was funded by the German Federal Ministry of Economics and Technology (BMWI 506 50EE1012/EnMAP) within the framework of EnMAP (Environmental Mapping and Analysis Program).

REFERENCES

1 Cocks T, R Jenssen, A Stewart, I Wilson & T Shields, 1998. The HyMapTM airborne hyperspectral sensor: the system, calibration and performance. 1st EARSEL Workshop on Imaging Spectroscopy *(*Zurich, Switzerland) pp. 37-42

2 Baastad I, T Løke & P Kaspersen, 2005. ASI - A new airborne hyperspectral imager. Proceedings of the 4th EARSeL Workshop on Imaging Spectroscopy - New Quality in Environmental Studies (Warsaw, Poland) pp. 107-110

3 Van der Meer F D, H van der Werff, F J A van Ruitenbeek, C A Hecker, W H Bakker,M F Noomen, M van der Meijde, E J M Carranza, J Smeth & T Woldai, 2012. Multi-and hyperspec-

tral geologic remote sensing: A review. International Journal of Applied Earth Observation and Geoinformation, 14, 112-128

4 Irons J R, J L Dwyer & J A Barsi, 2012. The next Landsat satellite: The Landsat Data Continuity Mission. Remote Sensing of Environment, 122, 11-21

5 Drusch M, U Del Bello, S Carlier, O Colin, V Fernandez, F Gascon, B Hoersch, C Isola, P Laberinti, P Martimort, A Meygret, F Spoto, O Sy, F Marchese & P Bargellini, 2012. Sentinel-2: ESA's Optical High-Resolution Mission for GMES Operational Services. Remote Sensing of Environment, 120, 25-36

6 Ungar S G, J S Pearlman, J A Mendenhall & D Reuter, 2003. Overview of the Earth Observing One (EO-1) mission. IEEE Transactions on Geoscience and Remote Sensing, 41, 1149-1159

7 Kaufmann H, K Segl, S Chabrillat, S Hofer, T Stuffler, A Mueller, R Richter, G Schreier, R Haydn & H Bach, 2006. EnMAP a hyperspectral sensor for environmental mapping and analysis. In: IEEE International Conference on Geoscience and Remote Sensing, 2006 (IGARSS 2006), 1617-1619

8 Pirajno F, 2009. Hydrothermal Processes and Mineral Systems (Springer-Netherlands) ISBN 978-1-4020-8612-0, 1250 pp.

9 Minnit R C A, 1986. Porphyrry Copper-Molybdenium mineralization at Haib river, South West Africa/Namibia. In: Mineral Deposits of Southern Africa, Volume I & II. C R Anhaeusser & S Maske, Eds. (Geological Society of South Africa: Johannesburg) Vol. 2, 1567-1585

10 Blignault HJ, 1977. Structural-Metamorphic Imprint on Part of the Namaqua Mobile Belt in South West Africa (Chamber of Mines Precambrian Research Unit; University of Cape Town: Cape Town)

11 Barr J M & D L Reid, 1993. Hydrothermal alteration at the Haib porphyry copper deposit, Namibia: Stable isotope and fluid inclusion patterns. Communications of the Geological Survey of Namibia, 8, 23-34

12 Oshigami S, Y Yamaguchi, T Uezato, A Momose, Y Arvelyna, Y Kawakami, T Yajima, S Miyatake & A Nguno, 2013. Mineralogical mapping of southern Namibia by application of continuum-removal MSAM method to the HyMap data. International Journal of Remote Sensing, 34, 5282-5295

13 Segl K, L Guanter, C Rogass, T Kuester, S Roessner, H Kaufmann, B Sang, V Mogulsky & S Hofer, 2012. EeteS - The EnMAP End-to-End Simulation Tool. IEEE Journal of Selected Topics in Applied Earth Observations and Remote Sensing, 5, 522-530

14 Mielke C, Y Fuchs, C Rogass, K Segl, F Pustlauck, O Blumenstein, H Kaufmann & M de Wit, 2012. The potential of spectroscopy to monitor mine waste and acid mine drainage in South Africa. 4th EARSeL Workshop on Remote Sensing and Geology (Mykonos Island, Greece 2012) 156-162

15 Mielke C, N K Boesche, C Rogass, H Kaufmann, C Gauert & M de Wit, 2014. Spaceborne mine waste mineralogy monitoring in South Africa, applications for modern push-broom missions: Hyperion/OLI and EnMAP/Sentinel-2. Remote Sensing, 6, 6790-6816

16 Chavez W X, 2000. Supergene oxidation of copper deposits: Zoning and distribution of copper oxide minerals. Society of Economic Geologists Newsletter, 41: 9-21

17 Kokaly, R F, 2012. Spectroscopic remote sensing for material identification, vegetation characterization, and mapping. In: Algorithms and Technologies for Multispectral, Hyperspectral, and Ultraspectral Imagery XVIII, edited by S S Shen & P E Lewis. Proceedings of SPIE, Vol. 8390

18 Abrams M, 2000. The Advanced Spaceborne Thermal Emission and Reflection Radiometer (ASTER): Data products for the high spatial resolution imager on NASA's Terra platform. International Journal of Remote Sensing, 21, 847-859

19 Clark R N, G A Swayze, R Wise, E Livo, T Hoefen, R F Kokaly & S J Sutley, 2007. USGS Digital Spectral Library, splib06a. U.S. Geological Survey Data Series; Rev. Sept. 2007 (U.S. Geological Survey: Denver, CO, USA) (last date accessed: 08 Dec 2014)